Available online at www.sciencedirect.com
SCIENCE DIRECT®
International Journal of Thermal Sciences 43 (2004) 849–864
International Journal of Thermal Sciences
www.elsevier.com/locate/ijts

Buoyancy-driven convection in two superposed fluid layers in an octagonal cavity

Sunil Punjabi, K. Muralidhar *, P.K. Panigrahi

Department of Mechanical Engineering, Indian Institute of Technology Kanpur, Kanpur 208 016, India

Received 3 March 2003; accepted 15 January 2004

Available online 27 March 2004

Abstract

Buoyancy-driven convection in a differentially heated cavity containing superposed layers of air–water, air–silicone oil and silicone oil–water has been experimentally studied. The apparatus is octagonal in plan. It has a nominal diameter of 130.6 mm and a height of 50 mm. The individual fluid layer heights have been kept equal to 25 mm in all the experiments. The cavity temperature difference has been varied over a range of 0.4 to 18 K, depending on the combination of fluid layers studied. Measurement of the thermal field in the octagonal cavity has been carried out using laser interferometry. Four different view angles namely 0, 45, 90, and 135° have been considered. The interface shapes have been recorded in the form of shadowgraphs. In the air–water experiments, the thermal fields in both fluid layers show a loss of axisymmetry, while progressing from a lower to a higher Rayleigh number. In air–oil experiments, a steady axisymmetric thermal field is observed in the oil layer, while a sufficient number of fringes did not form in air. In oil–water experiments, the thermal field in oil is close to axisymmetric. In water, the transition sequence to three dimensionality and unsteadiness is similar that of a single fluid layer. In most experiments, the cavity temperature difference is found to split across the fluid layers inversely in proportion to the effective thermal conductivity of the fluid layers. The experimental interface temperature matches the estimated value from single fluid correlations fairly well. Discrepancy with correlations is observed when the fluid layers are mechanically, rather than thermally coupled.

Keywords: Buoyant convection; Immiscible fluid layers; Heat transfer; Nusselt number; Interferometry

1. Introduction

Buoyancy-driven convection in differentially heated superposed fluid layers has been experimentally studied. The confining walls made of eight optical windows, form an octagon in plan. The fluid phases considered in the present work are air, water, and silicone oil. Experiments have been conducted with equal thicknesses of the fluid layers. The convection pattern in the cavity has been recorded using a laser interferometer. The flow field is visualized from four different view angles namely 0, 45, 90, and 135° when a pair of optical windows are aligned to allow the passage of the light beam. The positions of the laser and the CCD camera are held fixed during the experiments. The shape of the fluid–fluid interface has been imaged in the form of shadowgraphs. The objectives of the present work are to examine the nature of the axisymmetric thermal fields in the fluid layers, the influence of increasing Rayleigh number on transition to three dimensionality, and the appearance of unsteadiness. Temperatures attained at the interface, heat transfer rates at the walls in terms of Nusselt number and the nature of coupling between the two layers have also been investigated.

Important applications of flow and heat transfer in superposed fluid layers can be found in encapsulated crystal growth from its melt, growth of optical crystals from the aqueous solution [1], and buoyancy-driven convection in stratified water bodies such as a solar pond. The data from large aspect ratio, high Prandtl number experiments can be applied to study convection in the earth's mantle.

A linear stability analysis of buoyant convection in superposed fluid layers has been presented in [2]. The layer thicknesses were such that Marangoni effects were generally small. The interface deformation was included in the analysis, and a wide range of parameters was investigated. Conditions under which the onset of convection had viscous or thermal coupling, and exhibited Hopf bifurcation were determined. The theoretical predictions were compared with

* Corresponding author.
E-mail address: kmurli@iitk.ac.in (K. Muralidhar).

1290-0729/$ – see front matter
doi:10.1016/j.ijthermalsci.2004.01.007

Nomenclature

g	acceleration due to gravity	$m{\cdot}s^{-2}$
h	height of the fluid layer	m
H	height of the cavity	m
k	thermal conductivity	$W{\cdot}m^{-1}{\cdot}K^{-1}$
Nu	Nusselt number at the hot ($y=0$) and the cold wall ($y=H$), $=-(H/\Delta T)\frac{\partial T}{\partial y}\|_{y=0,H}$	
Pr	Prandtl number, $=\nu/\alpha$	
Ra	Rayleigh number, $=g\beta(T_{hot}-T_{cold})h^3/\nu\alpha$	
T	temperature	°C
T_{hot}	temperature of the bottom hot wall	°C
T_{cold}	temperature of the top cold wall	°C
T_i	interface temperature	°C
W	width of the cavity	m
y/H	non-dimensional vertical coordinate, measured from the average interface position	

Greek symbols

α	thermal diffusivity	$m^2{\cdot}s^{-1}$
β	coefficient of volume expansion	K^{-1}
μ	dynamic viscosity	$kg{\cdot}(m{\cdot}s)^{-1}$
ν	kinematic viscosity	$m^2{\cdot}s^{-1}$
ϕ	contact angle	
ρ	fluid density	$kg{\cdot}m^{-3}$
σ	surface tension	$N{\cdot}m^{-1}$
θ	nondimensional temperature, $=(T-T_{cold})/(T_{hot}-T_{cold})$	
ΔT	temperature difference across the cavity, $=(T_{hot}-T_{cold})$	K

experiments carried out in a rectangular cavity whose length was much greater than the cross-sectional dimensions. The fluids chosen were combinations of ethylene glycol–oil and ethylene glycol-decane. The measurement was based on the shadowgraph technique, with signals being recorded by a photodiode. The mode shapes realized in the experiments matched theory, though oscillatory convection and periodic switching of coupling modes were not experimentally verified. Pattern selection at the onset of instability in small aspect ratio containers with a free surface has been analyzed in [3]. The geometry considered was such that interface deformations were small, but in addition to buoyancy effects, Marangoni convection was significant. The analysis showed that the no-slip side walls greatly influenced the number of multiple stable patterns possible in comparison to free slip boundaries. Surface tension driven convection patterns in two liquid layers has been studied by Juel et al. [4]. Double-layer convection has been discussed from a theoretical and experimental viewpoint in [5], for geophysical applications. Experimental results for two immiscible fluid layers, driven by a vertical temperature difference slightly greater than critical for Benard instabilities have been reported in [6]. Both rectangular and annular cavities were considered. The conditions under which the onset of convection is time dependent was seen to be a function of the property ratio of the liquids constituting the fluid layers. A theory of secondary instabilities in liquid–gas system with a deformable interface was proposed in [7]. The flow field was taken to be driven exclusively by Marangoni convection, buoyancy effects being negligible because of the small layer heights. A wide variety of short and long-scale patterns were seen to be possible, in addition to the excitation of deformational waves at the interface. Experiments and numerical simulation for flow and thermal fields in the post-stability regime have been reported for rectangular cavities in [8,9].

In the context of crystal growth, two-layer convection has been studied in a cylindrical geometry by various authors. During liquid encapsulated crystal growth, the layer aspect ratio changes with time due to depletion of the melt. The effect of lateral boundaries on the flow pattern that arises when interfacial and gravity driven convection are present is an interesting aspect of two-layer convection. The effect of the container geometry on the flow pattern that forms near the onset of interfacial-driven convection has been studied in [10]. The numerical studies were carried out in a cylindrical geometry with two radius-to-height ratios of 1.5 and 2.5. The critical Marangoni numbers were calculated from the linearized Boussinesq equations, the interface deformations being assumed to be negligible. In continuation, the authors conducted experiments to study the effect of the layer height on the pattern formation in silicone oil–air system [11]. For flow visualization an infrared camera was used. The camera measured the infrared radiation emitted by the top surface of the silicone oil and thus the temperature distribution at the interface. The convection pattern set up in air was found to be quite weak to initiate mechanical coupling. However the thermal gradients were setup along the interface, leading to convection in the silicone oil layer due to buoyancy as well as surface tension gradients.

Extensive literature on convection in superposed miscible fluid layers (such as salt water and fresh water) is available. Instabilities characteristic of such systems include fingering patterns formed by the penetration of one fluid phase into the other. Both miscible and immiscible layers experience a wide range of flow regimes as a response to a very large parameter space of property ratios and dimensionless numbers [12].

In the present work, buoyancy-driven convection in differentially heated superposed immiscible fluid layers enclosed in an octagonal cavity has been experimentally studied. The fluid layers are horizontal with respect to the

direction of the gravity field. The fluid layer combinations considered in the present work are air–water, air–silicone oil, and silicone oil–water. The choice of these fluids is motivated by the fact that they are transparent, immiscible and have well-defined thermophysical and optical properties. The layer heights have been taken to be equal in all the experiments. The grade of silicone oil employed in the experiments was 50 cSt. Experiments have been conducted in the post-stability regime of buoyant convection in the fluid layers. Convection patterns in the cavity have been studied using a laser interferometer. The light beam orientation resulted in the depth-averaging of the respective thermal fields in the fluid layers. The recovery of the local temperature from its projections is possible using the principles of tomography [13].

Specific objectives of the present study are:

(1) to explore the similarities in the thermal fields in one layer and two-layer convection in the post-critical regime;
(2) nature of coupling between the fluid layers during energy transport;
(3) the applicability of single fluid correlations of heat transfer to superposed fluid layers; and
(4) the behaviour of interfaces, and the extent of their deformation.

Results have been presented in the form of the influence of Rayleigh number on the steady thermal field, interface temperature, and Nusselt number.

2. Apparatus and instrumentation

The test cell used to study buoyant convection in superposed fluid layers is shown in Fig. 1. It consists of three sections, namely the top tank, the test section (cavity) and the bottom tank. The test section is octagonal in plan and has a nominal diameter of 130.6 mm and a height of 50 mm. The cavity aspect ratio defined as the diameter-to-height ratio is 2.61; for the fluid layers, it is 5.22 for all the experiments. These values categorize the cavity as a small aspect ratio container [13].

The fluid layers, 25 mm thick are confined by two copper plates of thickness 1.6 mm above and below. The test cavity is essentially made of optical windows, 50 mm square and 3 mm thick, with 8 of them forming the octagon in plan. The windows are essential in the present work since they allow viewing of the thermal fields at parallel incidence and at various angles. For the octagonal geometry adopted for the experimental apparatus, view angles of 0, 45, 90, and 135° are possible. The optical windows are made of commercially available laser-grade fused silica. The high quality windows permit the passage of the laser beam without refraction. The optical windows were joined from outside by a mixture of hard-setting glue and grease. Thus,

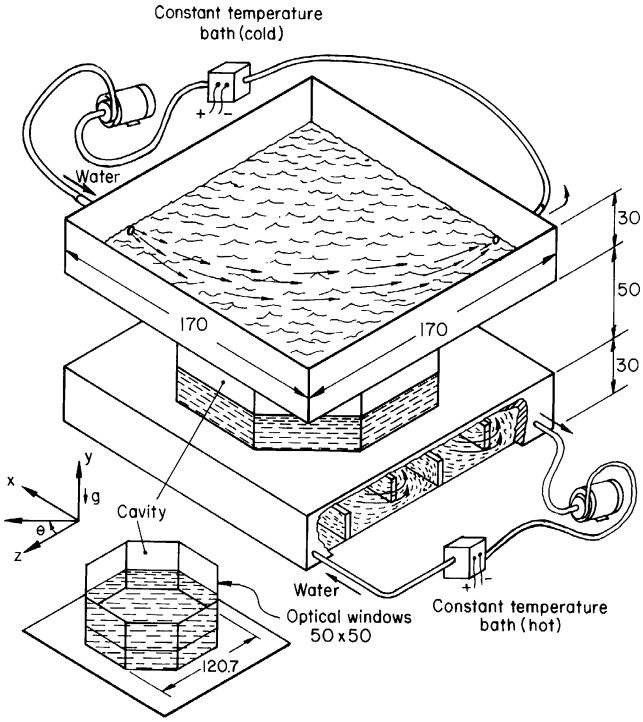

Fig. 1. Schematic drawing of an octagonal test cell to study convection in superposed fluid layers (all dimensions are in mm).

there were no disturbances to the field within the cavity, and leaks were successfully eliminated as well.

The hot and the cold surfaces have been maintained at uniform temperatures by circulating water from constant temperature baths (RAAGA and HUBER). A tortuous flow path has been created in the lower tank by installing 5 baffles, that additionally act as fins for the lower surface. On the lower tank, there is a natural tendency for the circulating water to form a free surface below the lower copper surface of the cavity. This necessitates the use of baffles that act as fins and maintain the temperature of the lower wall at the desired value. For the top tank, contact area between the flowing water and the copper surface was readily available. Both horizontal surfaces have been maintained at their respective temperatures to within ± 0.1 K, the tolerance of temperature control of the constant temperature baths. The wall temperatures were additionally monitored by several surface-mounted thermocouples connected to a multi-channel temperature recorder (SAN-EI). The surface areas of the two tanks have been designed to be much larger than the cavity to reduce edge effects.

To resolve near wall fringes, the two copper plates were carefully checked for flatness and surface finish. The flatness of the plates registered against a reference face plate was around 50 μm. The surface finish measured by an instrument (SURFANALYZER 5000) showed the RMS value to be close to 0.4 μm. During the experiments, the optical windows were additionally covered by 12 mm thick plexiglas in order to insulate the test section with respect

to the atmosphere. The plexiglas blocks of the opposite pair of optical windows are removed during data collection.

For measurements in liquids a reference chamber is required to be included with the interferometer to compensate for refractive index changes under isothermal conditions. The reference cell utilized in the present experiments is rectangular in construction. It is placed in the compensation chamber of the interferometer and is thermally inactive. By including the reference chamber, the interferograms reveal exclusively the variations in the thermal field in the cavity.

The apparatus is turned very slowly with the help of a traversing mechanism to record the interferometric projections at different view angles. To ensure that convection patterns are not influenced by this disturbance, a repeatability study was carried out over several days, as well as with slightly altered boundary temperatures. Other checks such as turning the apparatus in clockwise and counter-clockwise directions were also adopted. The results described in the present work were found to be reproducible in qualitative terms (for example, the deformation of the isotherms and the number of fringes). In quantitative terms, the local temperature profiles had an uncertainty level of $\pm 5\%$ when the longtime convection pattern was steady. In addition, the onset of unsteadiness was of the mode-switching type that was reproducible over the period when the experiments were carried out.

For temperature field measurement in the fluid medium, a Mach–Zehnder interferometer has been employed. It uses a 35 mW He–Ne laser (SPECTRA PHYSICS) and 150 mm diameter optics. Interferograms have been recorded using a CCD camera (PULNIX) that has a 512×512 pixel resolution. The camera is interfaced to an IBM-compatible PC through an 8-bit A/D card which digitizes the light intensity levels over the range of 0–255. Image acquisition is at video rates (50 images$\cdot$s^{-1}). Temperatures at various points over the solid surfaces of the cavity as well as the ambient temperature have been monitored by 18 gage K-type thermocouples. The thermocouples are in turn connected to a 30 channel recorder (SAN-EI) for the duration of the experiment.

Fringe formation in interferometry requires that the reference and the test beams are properly aligned. Thus a high degree of levelling of the test cell as well as the reference chamber with the interferometer optics is required. The test cell was levelled with respect to the laser beam, as well as other optical components. Since the apparatus rested on a machined surface that in turn was carried by a traversing mechanism, it was possible to level the interferometer with the test cavity and the reference chamber to an accuracy of better than 50 μm.

3. Experimental procedure

All experiments were conducted for 4–8 hours to confirm that steady state was reached in the fluid layers. Although, the flow field evolved fully in 2–3 hours, the experiment was continued for an additional 2–4 hours for detecting mild changes in the fringe field. In experiments where the fringe patterns had a displacement of less than 3–4 pixels, steady state was taken to have been attained. The time required for the thermal fields to reach steady state at the hot and the cold surfaces was found to be of the order of just a few minutes. With respect to the slow transients in the fluid media, the thermal loading of the two-layer system may be categorized as a step change. This information is required during numerical simulation with two fluid layers, the convection patterns and interface deformation of the present study being available for comparison.

4. Data analysis and uncertainty

The measurements of the thermal field were carried out in the infinite fringe setting of the interferometer. When a thermal disturbance is introduced in the path of the test beam, fringes appear in the field-of-view. The fringes represent contours on which the path integral of the temperature field along the direction of the light beam is a constant. The alignment of the interferometer in the infinite fringe setting was individually carried out for the fluid phases to capture the interferograms. For this purpose, the reference chamber was also filled with the fluid medium to be imaged. The reference chamber was however thermally inactive. The temperature drop per fringe shift, ΔT_ε can be calculated from principles of wave optics [14–16] as:

$$\Delta T_\varepsilon = \frac{\lambda / L}{\mathrm{d}n/\mathrm{d}T} \tag{1}$$

where λ is the wavelength of laser beam, $\mathrm{d}n/\mathrm{d}T$, the gradient of the refractive index with temperature is a fluid property, and L is the length of the test cell in the direction of the light beam. For the test cell of the present study, its length for all view angles (0, 45, 90, and 135°) remained equal. The temperature drop per fringe shift can be calculated from Eq. (1) as 5.65, 0.056 and 0.012 K respectively in air, water and silicone oil. Eq. (1) is applicable only when refraction errors are sensibly small. For experiments with large refraction errors, the interferograms have been qualitatively interpreted.

Several image processing operations are required before the interferograms can be interpreted in terms of temperature and the local heat transfer rates. The most important intermediate step is fringe thinning. It involves identification of the intensity minima within the fringe bands, for the entire image. Calculations for the temperature distribution, interface temperature, and Nusselt number have been performed using the thinned fringes. The instrumentation, image processing

and data analysis employed in the present work are similar to those reported in [17] for a single fluid. When interferograms are analyzed, we replace a fringe by an isotherm. Since the fringe is of finite thickness, it has to be collapsed to a curve of one pixel width, before a temperature value is assigned to it. This step is accomplished by using the point of minimum light intensity within the fringe band. The entire process is called *fringe thinning.*

Errors in the experimental data arise from the misalignment of the apparatus with respect to the light beam, image processing operations including filtering and thinning, and assigning temperatures to fringes. In view of a large value of ΔT_ε, the number of fringes in air was small. This difficulty was circumvented in oil and water. Errors related to refraction effects in water and silicone oil were found to be high for larger cavity temperature differences, and posed a limit on the range of Rayleigh numbers that could be studied. In contrast, the fluid–fluid interface location could be easily identified in a shadowgraph image even at high Rayleigh numbers. All experiments were conducted several times to establish the repeatability of the fringe patterns. In the event of mild unsteadiness, the dominant pattern that prevailed for the longest duration was recorded. For single fluid experiments, the plate-averaged Nusselt number has been found to be in good agreement with published correlations of [18]. Differences are to be expected with reference to superposed fluid layers since one of the boundaries in this configuration is a fluid interface.

The single fluid correlations employed in the present work are summarized below [18]:

$$Nu(\text{air}) = 1 + 1.44\left[1 - \frac{1708}{Ra}\right] + \left[\left(\frac{Ra}{5830}\right)^{1/3} - 1\right] \quad (2)$$

$$Nu(\text{water}) = 1 + 1.44\left[1 - \frac{1708}{Ra}\right] + \left[\left(\frac{Ra}{5830}\right)^{1/3} - 1\right] + 2\frac{Ra^{1/3}}{140}\left[1 - \ln\frac{Ra^{1/3}}{140}\right] \quad (3)$$

For silicone oil (50 cSt), the correlation of large Prandtl number fluids yields:

$$Nu(\text{silicone oil}) = 0.089Ra^{1/3} \quad (Pr \gg 1) \quad (4)$$

The above equations summarize a large body of experimental data for single fluid layers, and do not explicitly contain the aspect ratio as a parameter. Thus, the level of uncertainty associated with the correlation is large, and is specified to be ±20%. Thermophysical properties of air, water and silicone oil are required to evaluate the above equations. These are summarized in Table 1 at 25 °C, the ambient temperature maintained during the experiments.

When applied to superposed fluid layers, Rayleigh numbers in Eqs. (2), (3), and (4) are based on the temperature difference between the interface and the nearest solid boundary. Though the interface is not an isotherm, the maximum temperature variation over it was found to be smaller than 0.12 K, and hence negligible. Eqs. (2)–(4) can also be used to estimate the interface temperature by requiring that the energy transferred across one fluid layer is equal to that across the second, at steady state.

In air–water experiments, the Nusselt number matched the correlations of Eq. (3) in water to within ±7 and ±12%, respectively, at the lowest and highest Rayleigh numbers. The interface temperature matched the correlations within ±1.8% for all the Rayleigh numbers considered in the experiments. Nusselt numbers obtained at the hot wall for each of the view angles and Rayleigh numbers were within an error band of ±2%. In air–oil experiments, Nusselt number at the hot wall in oil and interface temperatures matched the correlations to within ±5 and ±0.5%, respectively, for the lower range of Rayleigh numbers. At the highest Rayleigh number, the uncertainty in measurements became quite high due to a very large number of fringes and high refraction errors. For a similar reason, quantitative analysis of fringes was not possible at high Rayleigh numbers in the oil–water experiment. In addition, the thermal field in water was found to become unsteady. In oil, the Nusselt number matched the correlations to within ±4%, while the interface temperatures were within ±0.5%.

To estimate the interface deformation due to surface tension, the formulation of [19] was adopted. The extent of deformation was found to be less than 10% of that seen in the experiments. Similarly, the temperature variation over the fluid–fluid interface being negligible, Marangoni convection was estimated to be of secondary importance as follows.

The temperature variation over the interface of the fluid layers can be found from the number of fringes that intersect this boundary. In most experiments, the number is restricted to one or two fringes. This corresponds to a temperature difference of $2 \times \Delta T_\varepsilon$ over the width of the cavity. In numerical terms, the maximum temperature difference is around 0.112 °C. The characteristic temperature difference can also be estimated in terms of heat flux as

$$\Delta T = 0.1\frac{q_{\max}}{k}d$$

Table 1
Thermophysical properties of air, water and silicone oil at 25 °C

Fluid	ρ [kg·m^{-3}]	ν [m^2·s^{-1}]	μ [kg·m^{-3}·s^{-1}]	k [W·m^{-1}·K^{-1}]	α [m^2·s^{-1}]	β [K^{-1}]	Pr
Air	1.184	15.5E–06	18.4E–06	26.1E–03	2.19E–05	3.35E–03	0.71
Water	997.05	89.3E–08	89.04E–05	0.611	1.46E–07	20.57E–05	6.1
Silicone oil	960	5.00E–05	4.80E–02	0.151	1.05E–07	1.06E–03	476.2

as described in [19]. The Marangoni number can be estimated as

$$Ma = \frac{\sigma_T \Delta T d}{\mu \alpha} = 11.2$$

This value is quite small, since a typical value that can influence the onset of convection is 79.6 [20,21]. Davis [22] has, however, pointed out that flow owing to a surface tension gradient can be established even at low Marangoni numbers. In the present study, one can expect Marangoni convection to influence buoyant convection, but as a higher order effect.

The images of the fluid–fluid interface were obtained without the reference beam. In effect, these images can be understood as shadowgraphs of the convection pattern. They can be approximately interpreted as the distribution of the Laplacian of the temperature field [15,16].

5. Results and discussion

Convection in horizontal superposed layers differs from that in a single layer mainly due to the formation of a well-defined interface. If one of the fluids is a gas, the interface could be a free surface, and the motion of the fluids could be practically uncoupled. When the fluids are placed in an enclosure and the motion is thermally driven, flow patterns in the fluid layers are coupled even when one of the phases is a gas. In a two-layer system, instabilities and convection patterns depend on several dimensionless groups. Specifically fluid property ratios, Rayleigh numbers of the individual fluid layers, layer thickness ratio, cavity aspect ratio and the overall geometry of the confining surfaces are important. Two distinct modes of flow coupling between the fluid phases via the interface are possible. These are thermal and mechanical coupling respectively. In thermal coupling, the recirculation patterns in the individual layers are driven by the temperature difference appropriate for each of them. It is thus possible for the rolls in each phase to have identical sense, clockwise or anti-clockwise. In mechanical coupling, the circulation in one phase drives that in the other by the mechanism of viscosity. Thus the two rolls can be oppositely oriented. Additional factors related to interface deformation, unsteadiness and three dimensionality generate quite a few possibilities, as the parameter range is explored.

The planform of the cellular pattern is determined by the shape of the apparatus. In the circular cavity, the rolls are expected to form concentric rings. Following [23], the possible roll formation in the circular test cell is as shown in Fig. 2(a). The octagonal test cell of the present experiments is different from the circular. In principle, corners can strongly influence the flow field. However, the corners are expected to play a less important role because the active surfaces that drive convection are the horizontal (top and bottom) boundaries. The side walls are thermally insulated and are essentially passive. Hence, to a first approximation, one can expect the results of the present study to be applicable to a circular cavity. In addition, the octagonal test cell has an advantage over the circular. In interferometry, a fluid layer cannot be viewed at normal incidence if the bounding walls are curved.

When a laser beam is used to image the thermal field in a rectangular cavity, the interferometric fringes align with roll pattern itself. Conversely, the roll pattern can itself be identified from the fringe displacement. For a circular cavity, the fringe field forms as a superposition of several rolls. It can be shown that for the roll pattern of Fig. 2(a), the fringes (namely, the contours of constant depth-averaged temperature) arrange themselves to form a symmetric Ω (omega) pattern. The full thermal field of the fluid layer is a collection of omegas (Ω) and inverse omegas (℧) interlinked with one another (Fig. 2(b)). Such patterns have also been noticed in experiments and calculations for buoyancy-driven convection in a large aspect ratio circular cavity filled with a single fluid [24], and has been reproduced in Fig. 2(c).

In the present work, the appearance of Ω-shaped fringes has been interpreted as being equivalent to an axisymmetric temperature field. The interferograms have been subsequently interpreted to understand the influence of increasing Rayleigh number on transition to three dimensionality and unsteadiness. In addition, the local temperature profiles, average interface temperature and wall Nusselt numbers have been determined. The thermal fields discussed below pertain to the convection patterns that form after the passage of the initial transients.

The temperature differences applied across the cavity are large enough for the Rayleigh numbers to be sufficiently greater than the respective critical values. In the experiments, straight fringes (corresponding to the conduction state) were seen at $Ra < 1707$, and deformed fringes for $Ra > 1707$. Thus, for the fluid combinations considered, convection can be taken to be induced in the respective layers at a Rayleigh number of around 1707, based on the individual layer heights and temperature difference. The degree of departure from criticality can be gauged in terms of the ratio $(Ra/Ra_{\text{critical}})$. The Rayleigh number corresponding to the individual fluid layers have been calculated in the following sections to present the level of criticality.

5.1. Air–water experiments

Fringe patterns in a cavity half-filled with water, the rest being air are presented in Fig. 3(a)–(d), respectively. The fields shown correspond to the size of a single optical window. The window dimension in the experiments was 41% of the nominal cavity diameter. View angles of 0, 45, 90, and 135° are considered. The interferograms were recorded after an experimental run time of 4 hours, when the thermal field was fully evolved and the fringe patterns were quite steady. The top and bottom surfaces have been maintained at the temperatures of 22.5 and 29 °C, respectively, leading to a temperature difference of 6.5 K across the cavity. The estimated interface temperatures based on Eqs. (2) and (3) has

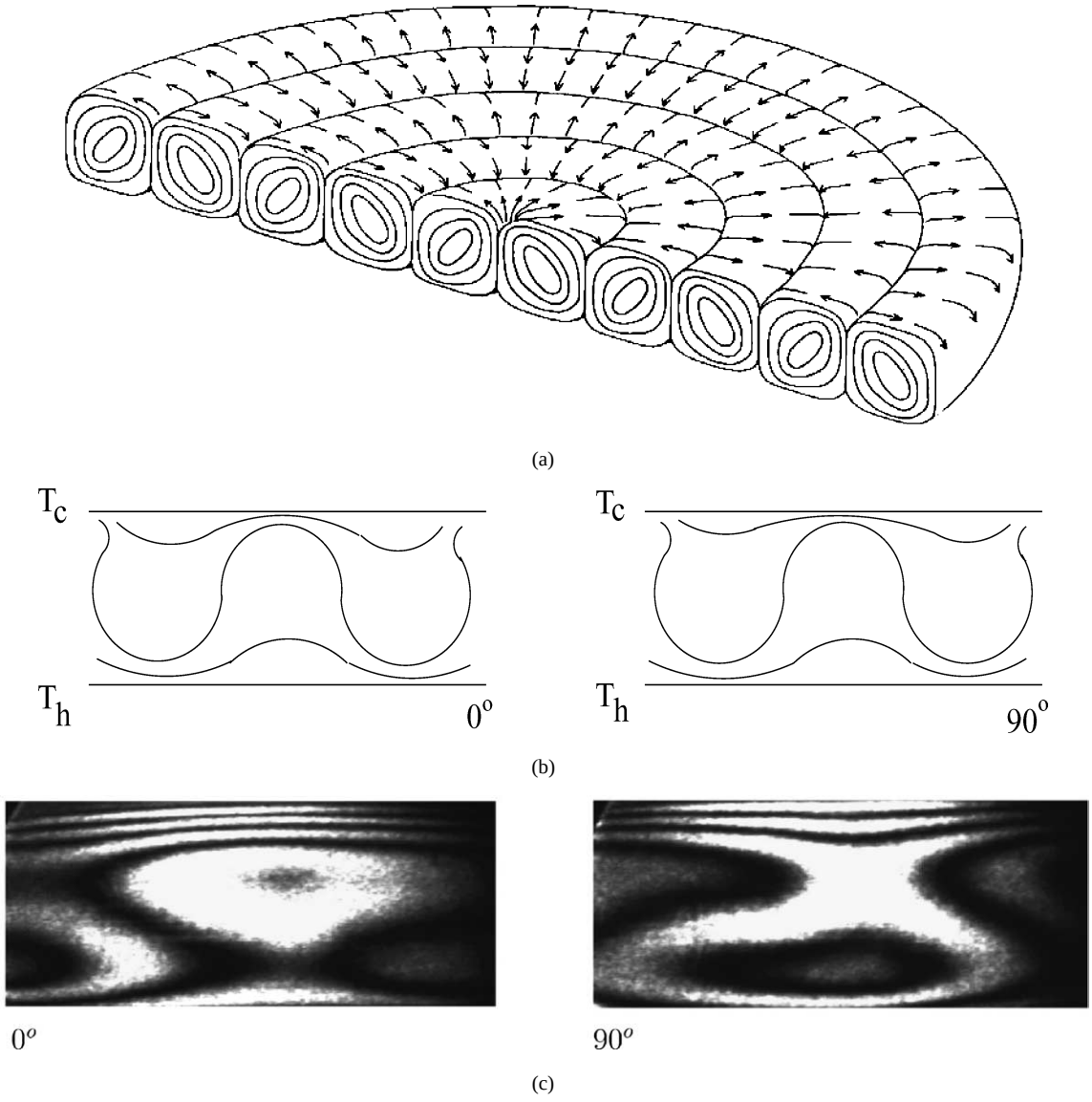

Fig. 2. Roll formation in (a) circular cavities, after Velarde and Normand [23], at moderate Rayleigh numbers and (b) idealized isotherms in orthogonal viewing of circular cavities corresponding to the roll in (a); (c) Omega-shaped fringes seen in an air-filled circular cavity (from [24]).

been obtained as 28.86 °C, while that based on the analysis of the interferometric images was 28.0 °C. The Rayleigh numbers in air and water can be calculated as 9 530 and 48 474, respectively. These are based on the estimated interface temperature. Fig. 3(a)–(d) show that the temperature distribution at different view angles appear to be similar in terms of orientation of the fringes, their number and spacing. Owing to similarity of fringe patterns with respect to the view angle, the thermal field may be expected to be axisymmetric. The fringes in the water phase are denser than in air, because its lower temperature drop per fringe shift. The few closed fringes in water are higher order fringes, and are related to interference of light rays that have a phase difference of an integer multiple of 2π. They have been ignored during fringe analysis.

A portion alone of the Ω pattern of fringes (Fig. 2(b)), characteristic of axisymmetric thermal fields is realized in the air and water phases of Fig. 3. It is because only a part of the cavity, corresponding to the size of the optical window has been imaged. With this factor taken into account, concentric rolls may be visualized in both air and water. In addition, the flow in each fluid layer is driven by the respective temperature difference between the nearest wall and the interface. Therefore, it can be concluded that the two layers are thermally coupled. High density fringes to be noticed near the air–water interface region in water, suggesting that the interface is thermally active. It is a consequence of a higher thermal conductivity of water compared to air, combined with a smaller value of the temperature drop per fringe shift. The fringe patterns of Fig. 3(a)–(d) can be utilised to evaluate the temperature field and Nusselt number variation at the walls of the cavity. These quantities are discussed in a later section.

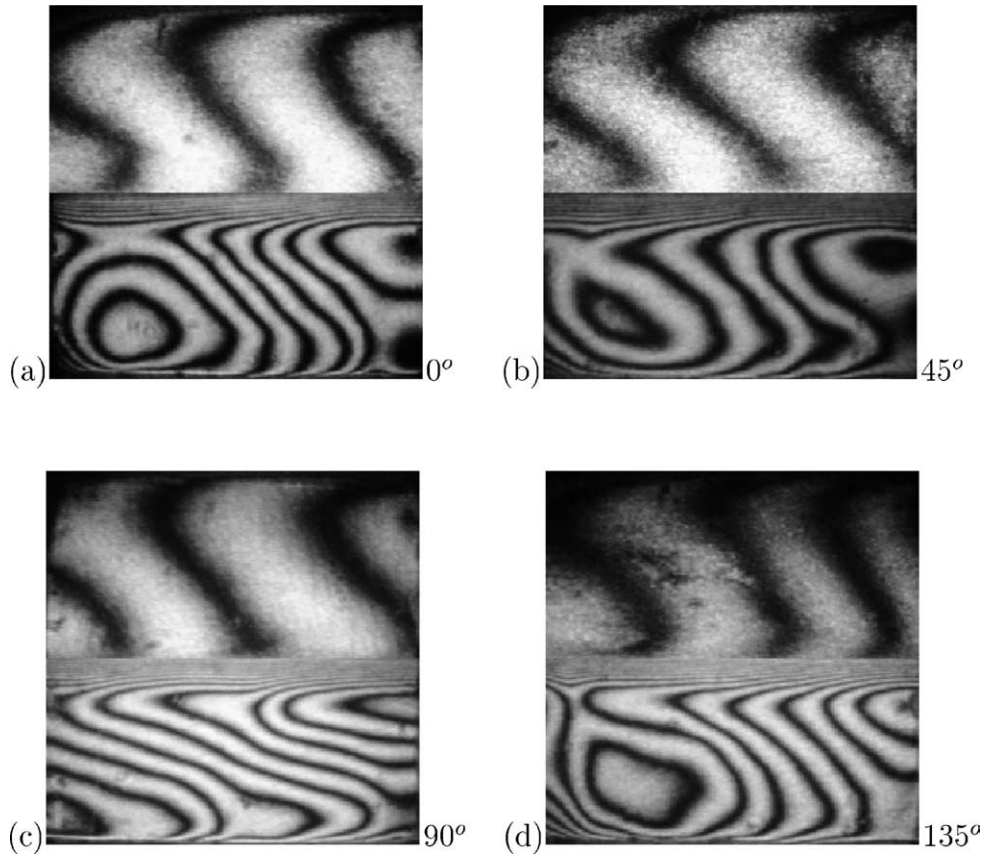

Fig. 3. Long-time interferograms obtained in a cavity filled with air and water for a temperature difference of 6.5 K. View angles are (a) 0°, (b) 45°, (c) 90°, and (d) 135°.

In Fig. 4(a)–(d), convection patterns for hot and cold wall temperatures of 30 and 21.5 °C are presented. The corresponding temperature difference is 8.5 K. The experimentally determined interface temperature and that estimated were calculated to be 28.66 and 29.72, respectively. Based on the estimated interface temperature, the Rayleigh numbers in air and water layers were calculated to be 12 466 and 66 992, respectively. Due to an increased Rayleigh number in both the fluids, some unsteadiness in the fringe patterns was observed. The long-lived dominant patterns have been recorded as a representative field in Fig. 4. Interferograms obtained in water at the four view angles show dissimilarity in terms of fringe orientation, number of fringes, and fringe spacing. The air phase exhibits a degree of similarity in terms of roll orientation and number of fringes. Thus, it may be concluded that the thermal field in the cavity is close to two-dimensional in air, but is three-dimensional in water. An increased number of closed higher order fringes in the water layer can be associated with higher temperature gradients and hence greater refraction within the fluid layer.

5.2. Air–silicone oil experiments

Experiments in a circular cavity containing superposed layers of air and silicone oil of equal thickness are discussed in the present section. For measurements, temperature differences of 1.8 and 3.1 K were applied across the cavity. For larger values, refraction errors were found to be significant in silicone oil. The temperature drop per fringe shift in air being 5.65 K, the above cavity temperature differences did not produce any fringe in the air portion of the cavity.

Fig. 5(a)–(d) show the thermal field in silicone oil for a cavity temperature difference of 1.8 K imposed across the cavity. The cold and the hot bounding surfaces have been maintained constant at 28.3 and 30.1 °C, respectively. View angles of 0, 45, 90, and 135° have been presented. The experimental and the estimated interface temperatures were 29.80 and 29.87 °C, respectively. Accordingly, the Rayleigh numbers can be determined to be 2237 and 6963 respectively in the air and oil. The Rayleigh number realized in oil is large enough for a clear convection pattern to be set up. The fringe patterns recorded were quite steady after 4 hours of experimentation. Dense fringes seen in oil near the interface are similar to those seen in the air–water experiments. Steady Ω-shaped isotherms, though with a distortion are obtained in the oil layer. The thermal field in oil can be broadly identified to be axisymmetric. High density fringes are noticed in silicon oil near the interface suggesting the interface to be thermally active. The flow inside the individual air and silicone oil layers is driven by the temperature difference

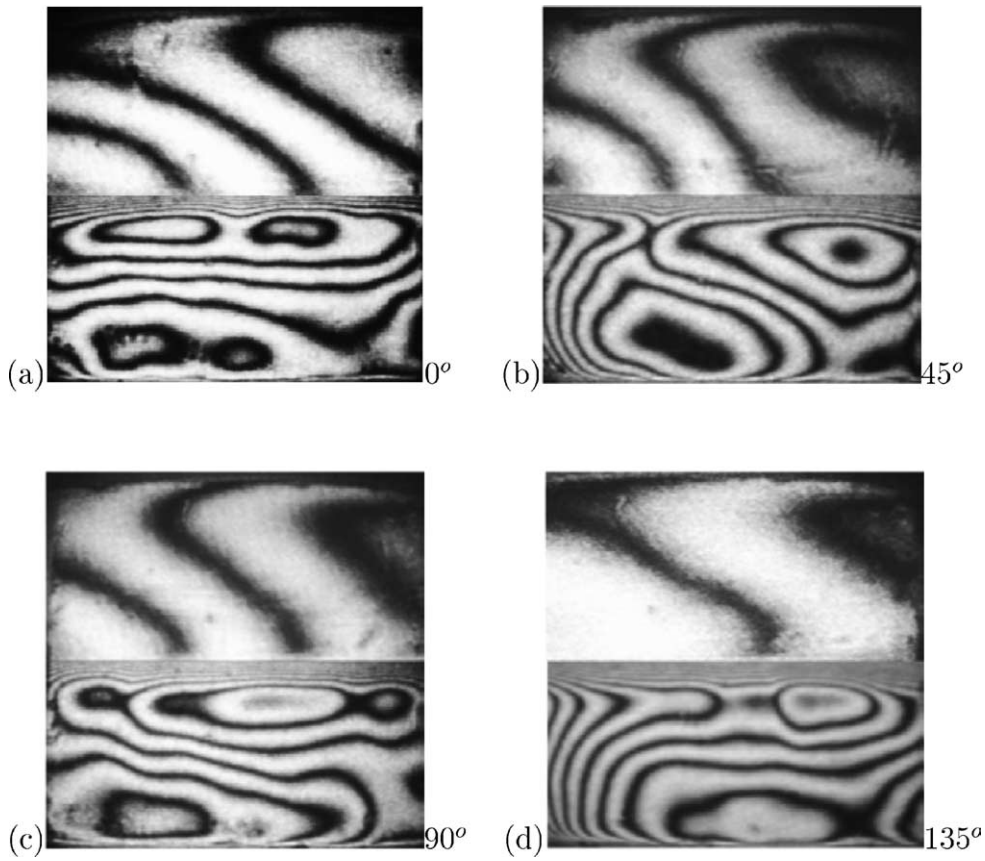

Fig. 4. Long-time interferograms obtained in a cavity filled with air and water for a temperature difference of 8.5 K. View angles are (a) 0°, (b) 45°, (c) 90°, and (d) 135°.

between the wall and interface and thus the fluid layers are thermally coupled.

For a imposed temperature difference of 3.1 K across the cavity, the fringe patterns obtained for view angles of 0, 45, 90 and 135° are shown in Fig. 6. At the end of four hours, the fringes in oil were quite steady with time. A single fringe appeared in the field-of-view of air near the cold wall owing to an increase in the temperature drop. The cold and the hot surfaces were maintained in the experiment at 27 and 30.1 °C, respectively. The interface temperatures were determined from the interferograms to be 29.70 and 29.76 °C for 0 and 90° view angles, respectively. The interface temperature estimated from energy balance has been found to be 29.68 °C. The Rayleigh numbers can be calculated as 3861 and 12 781 respectively in air and oil. With reference to the interferograms, fringes in oil reveal a practically axisymmetric thermal field.

5.3. Silicone oil–water experiments

Fig. 7(a)–(d) show interferograms for view angles of 0, 45, 90, and 135° at a cavity-imposed temperature difference of 0.4 K across the cavity. The cold and the hot bounding surfaces were maintained at temperatures of 29.7 and 30.1 °C, respectively. Based on the average of the two estimates from the oil and the water sides, the interface temperature has been calculated from the interferograms to be 29.93 °C for the 0° view angle; it is 29.9 °C for a view angle of 90°. The estimated interface temperature based on energy balance has been found to be 30.05 °C. The Rayleigh numbers in oil and water have been calculated as 10 955 and 17 266, respectively. Though the temperature drop in oil is slightly larger than that in water, a larger number of fringes appear in the field-of-view of oil owing to its smaller value of ΔT_{ε}, being 0.012 K as compared to 0.059 K for water. The flow field in oil was quite steady, while in water unsteadiness persisted even after the passage of a sufficient amount of time. The dominant pattern that prevailed for the longest fraction of time has been reported in Fig. 7.

In the oil layer, flow develops close to the cold wall in the form of an inverted omega (ʊ). Interferograms obtained at the four view angles in the oil layer are quite similar in terms of the fringe orientation, number of fringes, and fringe spacing. A greater degree of dissimilarity is realized in the water layer. Thus the fringe patterns in oil represent an axisymmetric field. In water, the projection data of view angles of 0 and 135° are similar, while the pair for 45 and 90° are also similar. Jointly, the field in water is however three-dimensional. Since the three dimensionality in water has not predominantly influenced the thermal field in oil, one can conclude that mechanical coupling between the layers is of secondary importance.

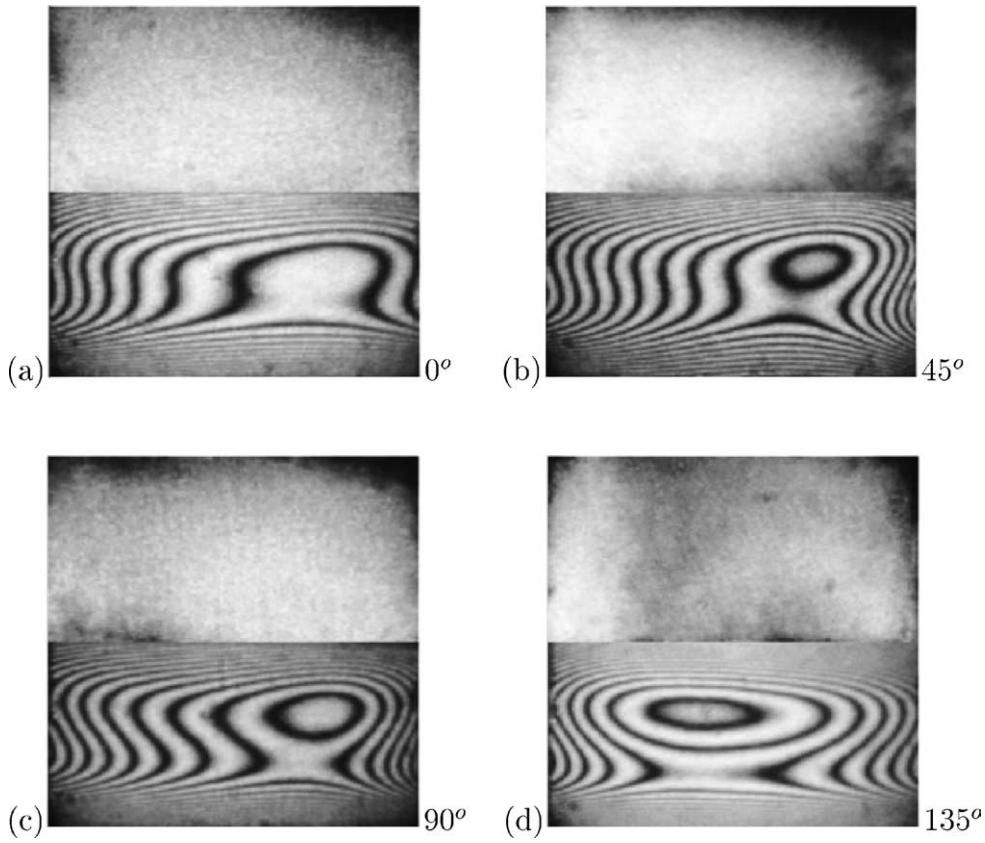

Fig. 5. Interferograms in a cavity filled with air and silicone oil; Cavity temperature difference is 1.8 K. View angles are (a) 0°, (b) 45°, (c) 90°, and (d) 135°.

Fig. 8(a)–(d) show the dominant fringe patterns formed in oil and water at a cavity temperature difference of 1.8 K. Data for the four view angles of 0, 45, 90 and 135° have been presented. The cold and the hot plate temperature are 28.3 and 30.1 °C. The interface temperatures have been calculated in the experiments to be 29.27 and 29.23, respectively, for view angles of 0 and 90°. The estimated interface temperature from correlations was 29.86 °C. The Rayleigh numbers of the individual fluids can be calculated to be 48 402 and 88 157 in oil and water respectively. A vigorous convective motion was observed in water due to a high Rayleigh number. Steady state was not obtained even after 7 hours of experimentation. However the fringe patterns in oil layer quickly reached a steady state. The inverted omega (℧) isotherms in the oil layer show distortion. This indicates the rolls to be in the form of steady concentric rings, though not axisymmetric. The thermal field in water, in contrast is unsteady and three-dimensional.

The flow in the individual fluid layer is seen to be dependent on the temperature difference between the nearest wall and the interface. The unsteadiness in the fringe patterns of water at the Rayleigh number is obtained, despite the stabilizing influence of silicone oil. This suggests the flow to be thermally rather than mechanically coupled at the interface. A later analysis of Nusselt number, however shows mechanical coupling to be present as well.

A further discussion on the joint coupling of fluid layers is required. All fluid layers are thermally as well as mechanically coupled. The former refers to continuity of heat flux at the interface. The latter refers to the combination of the no-slip condition and the continuity of shear stress. When the influence of one of the modes is localized in spatial extent, it appears as if the layers exhibit a single coupling. It is conceivable that shear at the interface has a local influence, while convection in the bulk of the fluid is buoyancy-driven. This is an example of thermal coupling. The classification in terms of the roll orientation in the individual layers is beneficial when one or the other mode is individually present.

The state of the flow field in the individual fluid layers and the respective Rayleigh numbers are summarized in Table 2. The data summarized here is broadly in agreement with regime map and the discussion of [25], in the context of convection in single fluids.

5.4. Steady state temperature profiles

The interferograms of Figs. 3–8 have been analyzed to determine the local temperature profile in the cavity. For definiteness, the cavity-averaged profiles have been presented in Fig. 9. Owing to few fringes appearing in air, the full temperature profile could not be plotted. The dashed-line shown in air is to be interpreted as an expected trend.

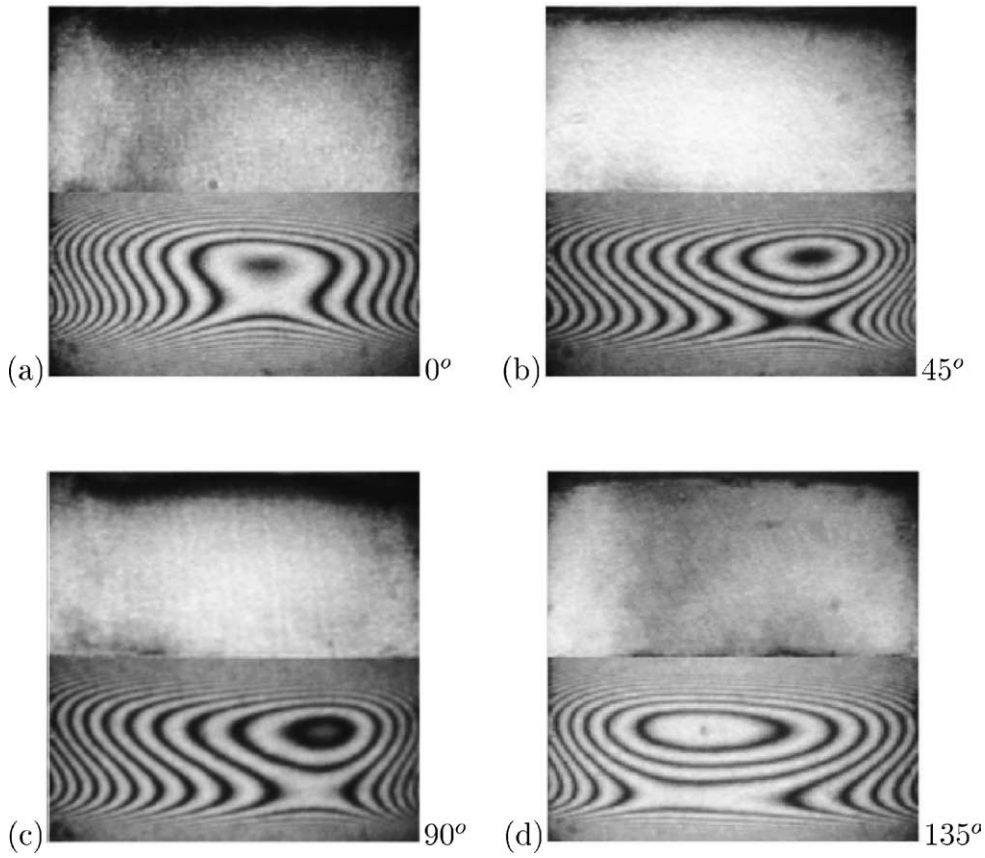

Fig. 6. Interferograms in a cavity filled with air and silicone oil; Cavity temperature difference is 3.1 K. View angles are (a) 0°, (b) 45°, (c) 90°, and (d) 135°.

Table 2
Summary of flow regimes and Rayleigh numbers recorded in the experiments. Thermal coupling is marked T, mechanical is M

Fluid	Rayleigh number	Axisymmetric	3D, steady	3D, unsteady	Coupling
Air	9 530	×			T
Water	48 474	×			T
Air	12 466	×			T
Water	66 992			×	T
Air	2 237	×			T
Oil	6 963	×			T
Air	3 861	×			T
Oil	12 781	×			T
Oil	10 955	×			T
Water	17 266		×		T
Oil	48 402		×		T, M
Water	88 157			×	T, M

For clarity, temperature profiles of only two view angles namely 0° and 90° have been shown. The dimensionless temperature profiles have been plotted as a function of the non-dimensionalised vertical distance (y/H), where the y-coordinate is measured from the fluid–fluid interface.

In the experiments involving air (Fig. 9(a)–(d)), it is evident that the largest temperature drop occurs in air, and only a smaller drop takes place in water and silicone oil. This result is observed because of a significant disparity in the gas and liquid thermal conductivities. With an increase in the cavity temperature difference, the flow fields in the respective fluids is intensified. The effect is stronger in the liquid medium, as compared to air. Thus, the effective thermal conductivity of the liquid that includes buoyant motion increases to a greater extent, when compared to air. This factor reduces the temperature drop across the liquid layer, and leads to an increase in the interface temperature simultaneously with the cavity temperature

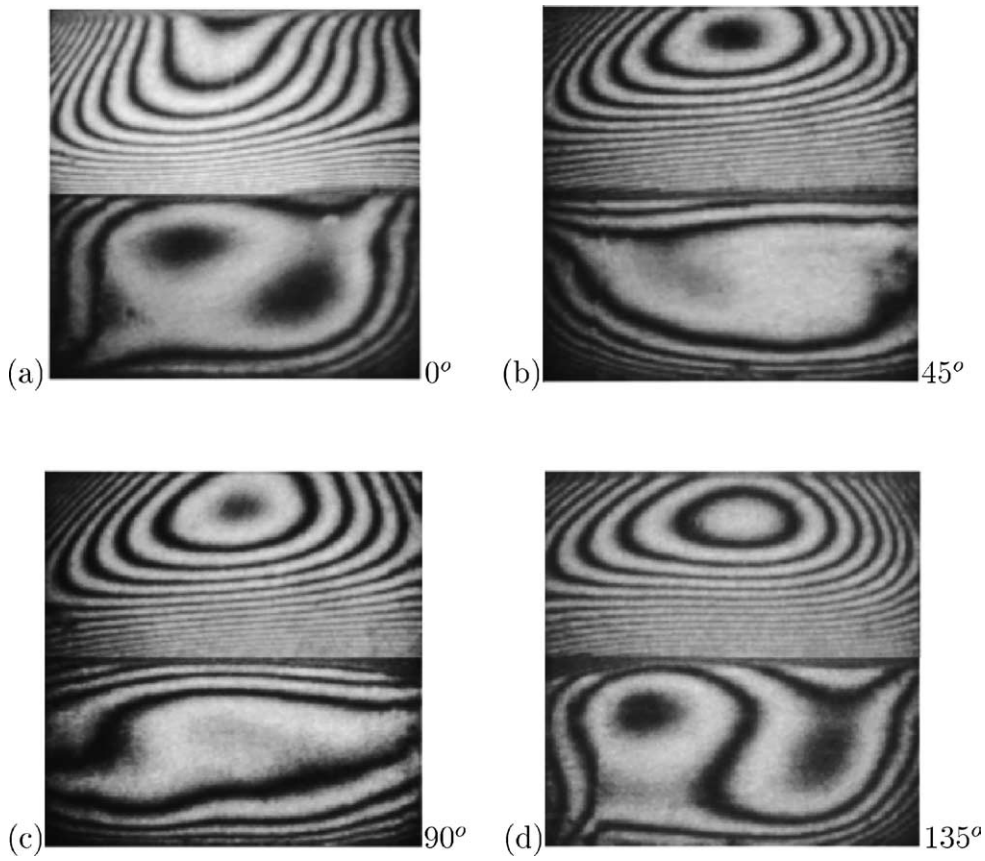

Fig. 7. Long-time interferograms in a cavity filled with silicone oil and water; Cavity temperature difference is 0.4 K. View angles are (a) 0°, (b) 45°, (c) 90°, and (d) 135°.

difference. The temperature profiles in the liquid media for the two view angles overlap, indicating a considerable degree of axisymmetry in the thermal fields.

Based on the fringe patterns of Figs. 7–8 for the oil–water experiments, the width-averaged temperature profiles in the two liquid phases are shown in Fig. 9(e)–(f). The thermal conductivity of oil is smaller than water by a factor of four, though larger than air by a factor of six. Despite the large difference in the thermal conductivities, a conclusion to emerge from Fig. 9(e)–(f) is that almost equal temperature drops occur in oil and water. This is because the layer Rayleigh numbers are quite high, and the effective conductivity and hence the heat transfer is convection-controlled. The interface temperature marginally increases with the cavity temperature difference. This result is understandable because of a sharp increase in the Rayleigh number in water (Fig. 9(f)), making the flow field three-dimensional as well as time-dependent. The width-averaged temperature profiles show a greater variability with the view angle in the oil–water experiments.

The appearance of dense fringes in silicone oil deserve comment: In the conduction regime, the fringes in oil are practically straight. When the convective rolls set in, the fringe density near the wall and the interface increase since the heat transfer rate across the cavity is now higher with respect to the conduction value. Fringe deformation is seen in the central portion of the oil layer where transport is advection-dominated. The dense fringes near the wall and the interface represent large temperature gradients and can be identified qualitatively as a diffusion boundary layer. With increasing cavity temperature difference, the layer Rayleigh number increases and the boundary-layer thickness decreases. Similar changes occur in air and water as well (in the axisymmetric regime), except that adequate number of fringes are not available for demonstrating the phenomena.

As discussed in [17], the determination of fringe temperatures is carried out simultaneously with the wall gradients. In the present work, the fringes were most clear at the fluid–fluid interface and occupied the full width of the cavity. Hence the gradients were calculated at this location. In air–water and air–oil experiments, Nusselt numbers have been determined in the liquid phase. Based on the local Nusselt number variation for each of the view angles, the width-averaged Nusselt number at the interface has been calculated. The interface temperature and the Nusselt numbers for view angles of 0 and 90° are in Tables 3–5. The Nusselt number for each fluid layer as determined from the correlations of [18] have been included for comparison. A factor that can cause differences between the measured Nusselt numbers and the correlations is the presence of a free-slip boundary in a superposed fluid configuration. Secondly, un-

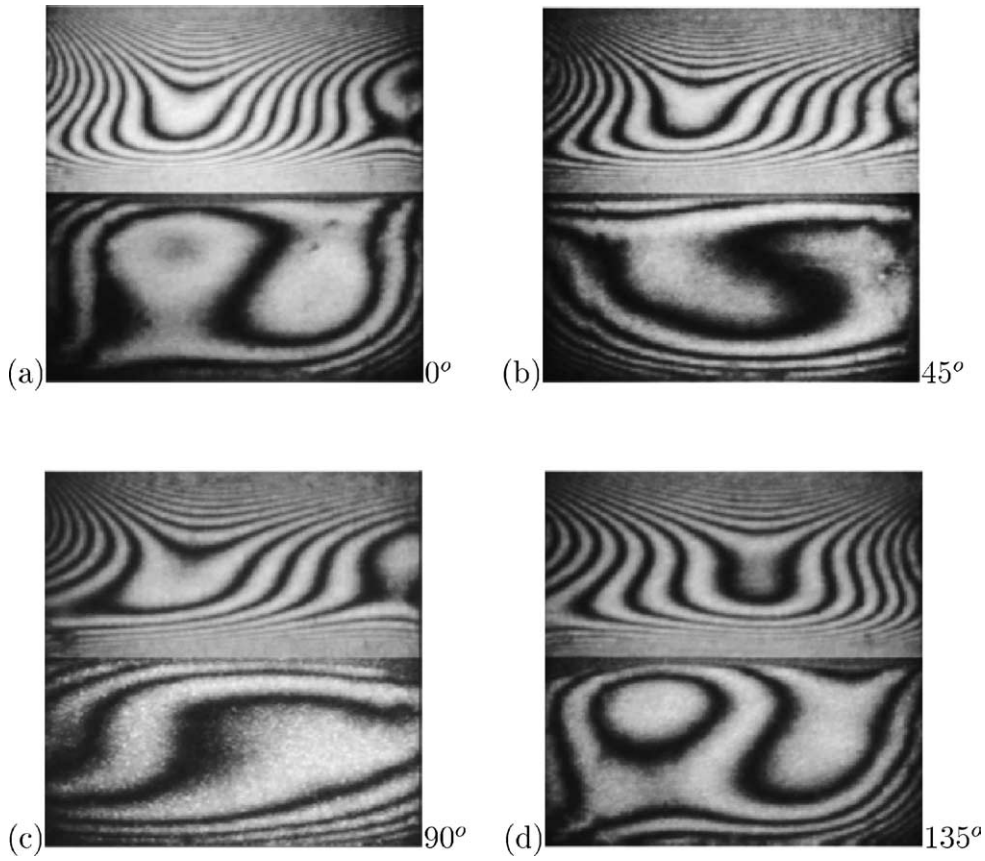

Fig. 8. Long-time interferograms in a cavity filled with silicone oil and water; Cavity temperature difference is 1.8 K. View angles are (a) 0°, (b) 45°, (c) 90°, and (d) 135°.

Table 3
Comparison of the interface temperature and Nusselt number with [18] in a cavity containing layers of air and water of equal thickness. View angle is marked 'V'

ΔT [K]	T_I (Expt) [°C]	T_I (Ref) [°C]	*Nu*		
			V-0°	V-90°	[15]
6.5	28.00	28.86	3.95	3.96	3.50
8.5	28.66	29.72	4.55	4.65	3.74

Table 4
Comparison of the interface temperatures and Nusselt numbers with [18] in a cavity containing layers of air and silicone oil of equal thickness. View angle is marked 'V'

ΔT [K]	T_I (Expt) V-0°	V-90°	T_I (Ref) [°C]	*Nu*		
				V-0°	V-90°	[19]
1.8	29.80	29.80	29.87	1.83	1.88	1.70
3.1	29.70	29.86	29.68	2.16	2.18	2.08

Table 5
Comparison of the interface temperatures and Nusselt numbers with [18] in a cavity containing layers of silicone oil and water of equal thickness. View angle is marked 'V'

ΔT [K]	T_I (Expt) V-0°	V-90°	T_I (Ref) [°C]	*Nu*		
				V-0°	V-90°	[19]
0.4	29.93	29.90	30.05	2.60	2.64	2.84
1.8	29.27	29.23	29.86	2.22	2.23	3.24

steadiness as well as three dimensionality in the flow are important since they are partially captured in the present experiments, while being fully averaged in the correlations.

Tables 3–5 show that the interface temperature predicted using the correlations match experiments quite well when the thermal field is steady. This result broadly agrees with the observation that the fluid layers in the experiments were thermally coupled. Discrepancies are seen when convection in the experiment is unsteady, as in the air–water experiment with a higher cavity temperature difference. A discrepancy is also to be seen in the oil–water experiment for $\Delta T = 1.8$ K, wherein convection in water is unsteady but is not as vigorous as required for a comparable Rayleigh number. The stabilizing of flow in water by the floating oil above is indicative of mechanical coupling between the layers, and a factor that reduces the Nusselt number. Thus, in the particular experiment being discussed, the layers are both thermally and mechanically coupled (Table 2). The single fluid correlations appear to be inadequate under these conditions.

5.5. Interface deformation

In the experiments discussed in the earlier sections, the fluid–fluid interfaces were practically flat. Interface deformation was first noticed in air–water experiments at high

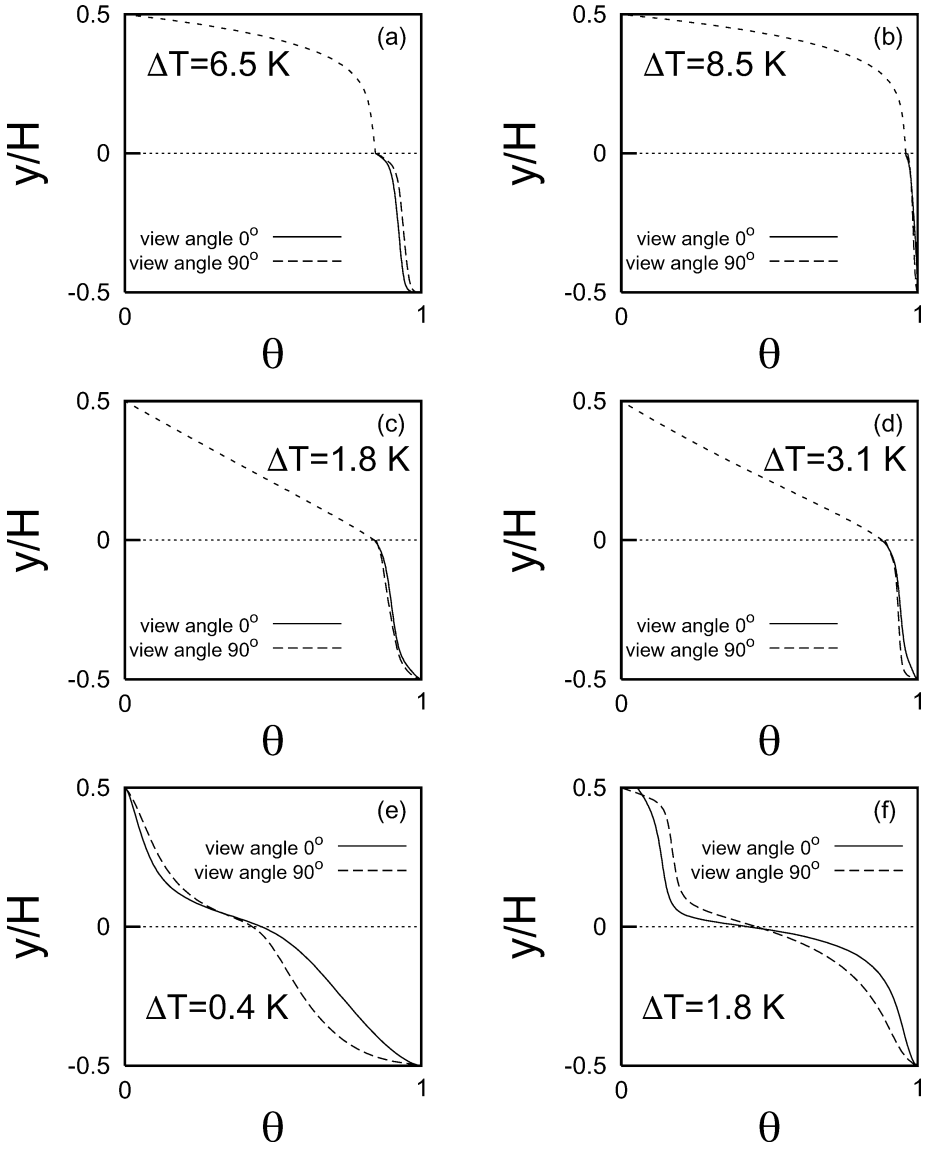

Fig. 9. Depth-averaged temperature profiles in a cavity filled with equal layer thicknesses of (a), (b) air and water, (c), (d) air and silicone oil, and (e), (f) silicone oil and water; Cavity temperature differences are 6.5 K and 8.5 K (a), (b), 1.8 K and 3.1 K (c), (d), and 0.4 K and 1.8 K (e), (f), respectively.

temperature differences, and hence Rayleigh numbers. Interferograms could not be captured at these Rayleigh numbers owing to large refraction errors. Instead, the interfaces could be detected in measurements carried out in the shadowgraph mode. In the present section, the deformation of the air–water interface has been discussed. The temperature difference across the cavity was 18 K in the experiments. The corresponding Rayleigh numbers in air and water were 27 068 and $1.72\text{E}+05$, respectively. The flow fields in both fluids were unsteady and three-dimensional. The interface showed up clearly when imaging focussed on the water layer, as opposed to air.

A time-sequence of interface movement in the air–water experiment is shown in Fig. 10(a)–(j). The images were recorded after convection in the cavity was fully established. Flow was seen to be fully evolved after the passage of around 4 hours. The time interval between successive interfaces in Fig. 10 is 1 minute. This is the time scale over which a significant change in the image was noticed. The vertical dimension in the individual images of Fig. 10 is 15 mm. The maximum interface deformation is of the order of 1–2 mm. There is a concentration of light intensity above the heated lower surface, leading to a practically bright patch in the images. A similar effect is to be seen in air as well, except that light refracts away from the cavity, leading to the formation of a dark patch. For preserving clarity, refraction effects in water alone have been shown. Below the interface, refraction effects at high temperature gradient locations result in the appearance of streaks of light that join the bright patch of light with the interface. The streaks are related to the circulatory motion of water in the cavity. Specifically, the streaks are to be expected at regions shared by adjacent rolls. Fig. 10 reveals the formation of several cellular structures in water, that form and break as a function

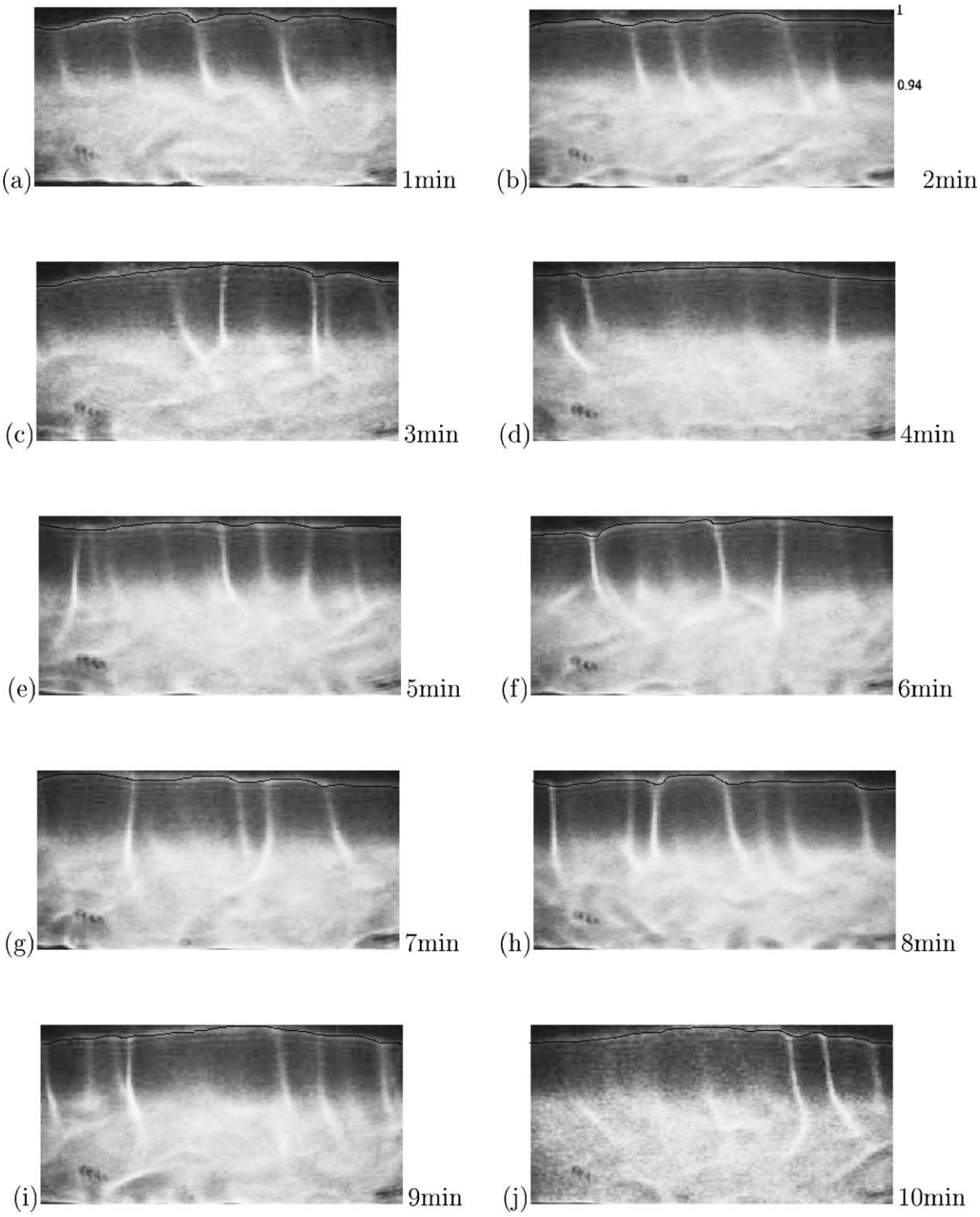

Fig. 10. Deformed interfaces in the cavity half-filled with water, the rest being air; $\Delta T = 18$ K; Time interval between two consecutive images is 1 minute. Interfaces are emphasized in black.

of time. The time sequence of Fig. 10 also shows that the light streaks bear a correlation to the change in curvature of the interface. Thus, the interface deformation originates in buoyant convection, rather than in surface tension or its gradients.

6. Conclusions

An interferometric study of convection in superposed layers of air, water, and silicone oil in the post-critical range of Rayleigh numbers was carried out. The following

conclusions have been arrived at in the present work.

In the cavity containing air and water, the fluid layers showed a degree of axisymmetry in the thermal field at a lower Rayleigh number. With an increase in Rayleigh number, three dimensionality was seen in water while axisymmetry persisted in air. In the air–oil experiments, omega-shaped fringe patterns indicating a steady two-dimensional thermal field was obtained in the oil layer over the range of Rayleigh numbers studied. In the oil–water experiments, the thermal field in oil was axisymmetric, while that in water was three- dimensional. At higher Rayleigh numbers, steady three-dimensional flow in oil (that is close to axisymmetric) and time-dependent three-dimensional flow in water were observed. The convective motion in each fluid layer was primarily driven by the individual temperature difference, indicating thermal coupling of the fluids at the interface. In oil–water experiments, a reduction in the strength of convection in water, revealed the simultaneous appearance of mechanical coupling.

The experimentally determined interface temperature matched the temperature estimated from single fluid correlations fairly well for all fluid combinations. The comparison in terms of Nusselt numbers was satisfactory. Discrepancy in the Nusselt number was seen at higher Rayleigh numbers in water owing to unsteadiness, and in oil–water experiments due to the stabilizing effect of the oil layer.

The deformation of the fluid–fluid interface was uniformly small in all the experiments. In an air–water experiment at high Rayleigh numbers, the shape of the interface correlated well with the position of the light streaks in a shadowgraph. The deformation could then be related to buoyant convection in air and water, rather than gradients in surface tension.

References

[1] N.A. Booth, A.A. Chernov, P.G. Vekilov, Characteristic lenghtscales of step bunching in KDP crystal growth: In situ phase shifting interferometry study, J. Crystal Growth 237–239 (2002) 1818–1824.
[2] S. Rasenat, F.H. Busse, L. Rehberg, A theoretical and experimental study of double-layer convection, J. Fluid Mech. 199 (1989) 519–540.
[3] H.A. Dijkstra, On the structure of cellular solutions in Rayleigh–Benard–Marangoni flows in small-aspect-ratio containers, J. Fluid Mech. 243 (1992) 73–102.
[4] A. Juel, J.M. Burgess, W.D. McCormick, J.B. Swift, H.L. Swinney, Surface tension-driven convection patterns in two liquid layers, Physica D 143 (2000) 169–186.
[5] F.H. Busse, G. Sommermann, Double-layer convection: A brief review and some recent experimental results, in: Y.Y. Renardy, A.V. Coward, D.T. Papageorgiou, S.-M. Sun (Eds.), Advances in Multi-Fluid Flows, SIAM, Philadelphia, PA, 1996, pp. 33–41.
[6] C.D. Andereck, P.W. Colovas, M.M. Degen, Observation of time-dependent behaviour in the two-layer Rayleigh–Benard system, in: Y.Y. Renardy, A.V. Coward, D. Papageorgiou, S.M. Sun (Eds.), Advances in Multi-Fluid Flows, SIAM, Philadelphia, PA, 1996.
[7] A.A. Golovin, A.A. Nepomnyashchy, L.M. Pismen, Nonlinear evolution and secondary instabilities of Marangoni convection in a liquid–gas system with deformable interface, J. Fluid Mech. 341 (1997) 317–341.
[8] A. Prakash, J.N. Koster, Steady Rayleigh–Benard convection in a two-layer system of immiscible liquids, Trans. ASME J. Heat Transfer 118 (1996) 366–373.
[9] A. Prakash, K. Yasuda, F. Otsubo, K. Kuwahara, T. Doi, Flow coupling mechanism in two-layer Rayleigh–Benard convection, Experiments Fluids 23 (1997) 252–261.
[10] D. Johnson, R. Narayanan, Experimental observation of dynamic mode switching in interfacial–tension–driven convection near a codimension-two point, Phys. Rev. E 54 (4) (1996) 3102–3104.
[11] D. Johnson, R. Narayanan, P.C. Dauby, The effect of air height on the pattern formation in liquid–air bilayer convection, in: Fluid Dynamics at Interfaces, Cambridge University Press, Cambridge, 1999, pp. 15–30.
[12] Y.Y. Renardy, C.G. Stoltz, Time-dependent pattern formation for convection in two layers of immiscible liquids, Internat. J. Multiphase Flow 26 (11) (2000) 1875–1889.
[13] K.R. Kirchartz, H. Oertel Jr, Three-dimensional thermal cellular convection in rectangular boxes, J. Fluid Mech. 192 (1988) 249–286.
[14] F. Mayinger (Ed.), Optical Measurements: Techniques and Applications, Springer, Berlin, 1994.
[15] R.J. Goldstein (Ed.), Fluid Mechanics Measurements, Hemisphere, New York, 1983, second ed., 1996.
[16] G.S. Settles, Schlieren and Shadowgraph Techniques, Springer, New York, 2001.
[17] D. Mishra, K. Muralidhar, P. Munshi, Interferometric study of Rayleigh–Benard convection at intermediate Rayleigh numbers, Fluid Dynamics Res. 25 (5) (1999) 231–255.
[18] B. Gebhart, Y. Jaluria, R.L. Mahajan, B. Sammakia, Buoyancy-Induced Flows and Transport, Hemisphere, New York, 1988.
[19] W. Shyy, H.S. Udayakumar, M.M. Rao, R.W. Smith, Computational Fluid Dynamics with Moving Boundaries, Taylor and Francis, New York, 1996.
[20] P.C. Dauby, G. Lebon, Linear Benard–Marangoni instability in rigid rectangular containers, J. Fluid Mech. 329 (1996) 25–64.
[21] D.A. Edwards, H. Brenner, D.T. Wasan, Interfacial Transport Processes and Rheology, Butterworth–Heinemann, New York, 1991.
[22] S.H. Davis, Thermocapillary instabilities, Annual Rev. Fluid Mech. 19 (1987) 403–435.
[23] M.G. Velarde, C. Normand, Convection, Scientific Amer. 243 (1) (1980) 79–94.
[24] A. Srivastava, P.K. Panigrahi, A combined numerical–experimental study of convection in an axisymmetric differentially heated fluid layer, Indian J. Engrg. Materials Sci. 9 (2002) 448–454.
[25] R. Krishnamurti, Some further studies on the transition to turbulent convection, J. Fluid Mech. 60 (1973) 285–303.